

THE *K2* LIGHT CURVES AND STUNTED OUTBURSTS OF AC CNCE. M. SCHLEGEL^{1,2} & R. K. HONEYCUTT³
Draft version April 10, 2019

ABSTRACT

We describe two observations of the nova-like cataclysmic variable AC Cnc obtained with *Kepler* during its revamped second mission (*K2*). Using the *K2* 1-minute cadence mode, the data were obtained during Campaigns 5 and 18. Campaign 5 (C05) lasted from \sim 2015 Apr 27 to \sim 2015 July 10, a total of 74.8 days, and yielded \sim 106,000 measurements. Campaign 18 (C18) lasted from \sim 2018 May 13 to \sim 2018 July 2, a total of 50.7 days, yielding \sim 72,000 measurements. The C05 light curve reveals two ‘stunted outbursts’ having properties consistent with stunted bursts observed from the ground; a stunted burst was underway during the C18 observation when it ended. During a stunted outburst, the primary eclipse is found to increase in depth but the residual brightness at mid-primary-eclipse remains nearly constant. By contrast, the secondary eclipse retains the same depth but the brightness at mid-secondary eclipse increases during outburst, following the orbital variations of the out-of-eclipse light. The eclipse ephemeris is statistically consistent with historical ephemerides and shows only marginal evidence for a period change. On the basis of the *K2* data, we can not confirm a previously-reported non-orbital periodicity in AC Cnc.

Subject headings: stars: individual (AC Cnc) – stars: novae, cataclysmic variables – (stars:) binaries: eclipsing

1. INTRODUCTION

Cataclysmic variables (CVs) are inherently variable objects, ranging from the outbursts of novae, recurrent novae, and dwarf novae to the flickering observed in disk systems. Understanding the causes of the variability requires disentangling the contributions of at least four sources: the white dwarf, its accretion disk, the mass transfer stream, and the red dwarf secondary.

Uninterrupted observations have led to several advances in our understanding of CVs and white dwarfs (WDs) (e.g., Patterson (2012); Provencal et al. (2014)). Such observations provide a context for variability, separating short-term variations from slower long-term trends.

In this paper, we describe observations of the novalike CV AC Cnc obtained during the *K2* portion of the *Kepler* satellite program. The *K2* mission was initiated by losses of gyros, which prevented the spacecraft from maintaining a stable pointing using the original guiding/pointing techniques employed earlier in the mission. *Kepler*, or *K2*, has a 95-cm diameter mirror and has two operational modes: 1- and 30-minute observational cadences. The spectral response function covers \sim 450 – 850 nm, hence it is a ‘white light’ telescope and detector.

AC Cnc has an orbital period of \sim 432.7 min = \sim 0.300 day and an eclipse depth of \sim 1.5 mag in the optical. We now briefly summarize studies of AC Cnc since its discovery by Kurochkin & Shugarov (1980) in 1980. Shugarov (1981) argued that AC Cnc was an old nova. Downes (1982) detected the secondary star through its G band and Mg *b* absorption features, pointing to a late G or early K star. Based on their observations, Yamasaki, Okazaki, & Kitamura (1983) inferred a large accretion disk with a steep brightness distribution.

Schlegel et al. (1984) collected time-resolved emission

line spectroscopy and obtained a mass ratio of \sim 1.24 \pm 0.08 from measured radial velocity curves of both stars. The radial velocity curve of the secondary was based on measurements of the G band absorption and led to a mass of $M_2 \sim$ 1.02 \pm 0.14 M_\odot . The radial velocity curve of the primary was measured using several emission lines and led to a mass $M_1 \sim$ 0.82 \pm 0.13 M_\odot .

Torbett & Campbell (1987) claimed a radio detection at 6 cm but K rding et al. (2011) could not confirm the detection in a re-analysis of the data. Dmitrienko (1995) carried out UBVRI photometry over a 4-year interval, noting that most of the variability in the 5-band photometry likely arose from changes in the state of the accretion disk, and discussed evidence for a reflection effect in the R and I band photometry.

Thoroughgood et al. (2004) presented time-resolved photometry and spectroscopy of AC Cnc. They also measured radial velocity curves of both stars. They obtained masses $M_1 = 0.76 \pm 0.03 M_\odot$ and $M_2 = 0.77 \pm 0.05 M_\odot$ for the secondary. The corresponding mass ratio is $q = 1.02 \pm 0.04$. Their primary mass lies within the uncertainties of the Schlegel et al. (1984) result; their secondary mass is lower by \sim 30%; the uncertainties of that mass from the two studies overlap at \sim 2 σ . These authors also inferred an inclination of $75^\circ.6 \pm 0^\circ.7$.

Finally, Qian et al. (2007) assembled all of the times of minima reported in the literature as well as contributing their own measurements. They reported detection of an orbital period change, arguing that it was evidence of magnetic braking and a second companion.

This paper describes two pointings of the eclipsing nova-like CV AC Cnc using the *Kepler* telescope in the short-cadence mode. Here we summarize the data and the stunted outbursts observed.

¹ Department of Physics and Astronomy, University of Texas-San Antonio, San Antonio, TX 78249; eric.schlegel@utsa.edu

² Vaughan Family Professor

³ Department of Astronomy, Indiana University, Bloomington, IN 47405; honey@indiana.edu

2. OBSERVATIONS AND DATA REDUCTION

Two data sets of AC Cnc were obtained using *K2*. For the first, *K2* observed the field of AC Cnc from 2015 April 27 \sim 02 UT (JD 2457139.6006) to 2015 July 10 \sim 22 UT (JD 2457214.44228) at a one-minute cadence during Campaign 5 (C05). The data were processed by the *K2* mission center and became available in November 2015.

For the second, campaign 18 (C18) lasted from \sim 2018 May 13.03 to \sim 2018 July 2.92, again at one-minute cadence for AC Cnc. These data were also processed by the *K2* mission center and became available in mid-November 2018. A total of \sim 50.7 days \sim 169 orbits were covered. C18 was truncated by a ‘hiccup’ in the fuel pump that occurred on 2018 July 2. In response, the *K2* operations team ended the campaign to preserve the data already collected.

Hereafter, instead of referring to specific orbits with ‘data set 1, orbits x to y’, we will abbreviate that phrase as ‘orbits 1:x-y’ or ‘2:a-b’. A similar construction will be used for other data set-related quantities.

For both data sets, we sifted through the short-cadence data using the basic software routines of Still & Barclay (2012), otherwise known as PyKE, looking for artifacts as described in Kinemuchi et al. (2012) as well as those identified by the *Kepler* Science Center. We first used the `keppixseries` to plot all of the data for each pixel (Figure 1). This demonstrated to us that the programmatically-defined aperture captured the vast majority of the events from AC Cnc with minimal or zero contamination from other stars. That conclusion is supported by an examination of a B band image of AC Cnc (DSS2, skyview.gsfc.nasa.gov) that shows just two stars in the immediate region of AC Cnc: one is North by \sim 5 *Kepler* pixels while the other is South by \sim 5-6 pixels. Those fortuitous stellar positions leave the light from AC Cnc uncontaminated to a high degree. Consequently, we did not apply any filtering to the data at this stage.

Short gaps occur in the data, usually lasting <0.005 in phase for data set 1, but longer for data set 2. Generally, the short gaps are associated with cosmic ray hits, data dumps, and attitude corrections. During C18, there are the usual cosmic ray hit-generated gaps. But there are also a number of small gaps as the spacecraft dropped into ‘coarse pointing’ rather than fine pointing, then re-gained fine pointing control. The longest gap occurs at orbits 2:46-47, when little data are collected during a gap lasting nearly a full orbit. We do not make any attempt to fill in gaps.

The short-cadence data then contains 1:109,890 and 2:73,728 individual points. We filtered both data sets to eliminate observations for which the SAP_QUALITY flag was non-zero, as recommended by the *K2* team. Cosmic ray hits and coarse pointing times comprised the bulk of the non-zero SAP_QUALITY flags. After filtering, the data sets had a total of 1:106,703 individual points covering the 74.8 days of the pointing and 2:72,549 points covering 50.7 days. Given that the period of AC Cnc is ≈ 0.3 days, we consequently expect $\approx 1:240$ -250 and $\approx 2:175$ successive eclipses; we count 1:246 and 2:169 eclipses.

2.1. Observational Precision

The photometric precision is limited by spacecraft jitter, demonstrated to be only a few percent larger than during the *Kepler* core mission, and the much larger solar wind-induced drift, which moves the source across pixels of varying sensitivity (Howell et al. 2014). In that paper, the photometric accuracy is presented as median 6-hour precision in parts per million (ppm), showing that the *K2* mission is about a factor of ≈ 4 worse than for the *Kepler* core mission – instead of ~ 20 ppm at mag 12, *K2* delivers ≈ 80 ppm.

However, the median 6-hour precision is not helpful given that our AC Cnc data sets have 1-minute cadence. A more direct measure of precision is available in Howell et al. (2014) who re-observed the transiting exoplanet WASP-28b, demonstrating 0.16% precision. If we then degrade that precision to a mag 13.5 object, we expect observations of AC Cnc at 1-minute cadence to possess $\approx 0.5\%$ precision. Consequently, for an observation yielding 10,000 counts, we expect $\lesssim 50$ counts of uncertainty. This is a factor of ≈ 1.5 above the uncertainties included in the *K2* data file. The variations in the light curve we describe are all substantially larger than these uncertainties.

As an aid to the reader, while we have not converted the data points to magnitudes, we could do so using the relation from the *Kepler* team between *K2* counts and magnitude:

$$f_{kep}/1.74 \times 10^5 = 10^{-0.4(K_{p2} - 12)}$$

or

$$K_{p2}(mag) = -2.5 \log(f_{kep}) + 25.10137.$$

where f_{kep} are the *K2* counts.

2.2. The Ephemeris

We define the minimum of each eclipse by fitting, for each eclipse, times $\approx \pm 15$ min about the approximate eclipse minimum with a second-order polynomial. These times of minima are then fit with the standard ephemeris equation to yield the period. Our initial ephemeris is then

$$BJD = 2457139.32155(\pm 24) + 0^d.300482312(\pm 15) \times E$$

where the uncertainties are in the last two digits.

The *Kepler* program returns times as BJD while all previous observations of AC Cnc are HJD (q.v. Qian et al. (2007) for the most up-to-date list of eclipse minima). As noted by Eastman et al. (2010), the difference between HJD and BJD is a semi-sinusoid with an amplitude up to ± 4 seconds $\sim 0^d.46 \times 10^{-4}$ for an object in the ecliptic plane. The sinusoid is primarily caused by the changing positions of Jupiter and Saturn. AC Cnc’s ecliptic latitude is $\sim 5^\circ$, which has negligible effect on that sinusoidal amplitude for our purposes.

While differences of a few seconds are small with respect to the $\sim 0^d.005$ (O - C) trend displayed in Qian et al. (2007), the differences are *not* small relative to the uncertainties of the times of minima. We presume the period and \dot{P} terms are relatively independent of the time references used. We therefore fit the data three times: firstly, we fit the two *K2* datas sets independently to verify that

we had the correct cycle count and to check for a \dot{P} term over the ~ 3000 orbits between C05 and C18. Secondly, we fit the combined *K2* data and the HJD data sets, for which we permitted the ephemeris start times and the \dot{P} terms to be independent, but set the orbital period to be simultaneously fit for the HJD and BJD data sets. Finally, we set the \dot{P} term equal between the HJD and BJD data sets and fit for the ephemeris start time and period.

The results are shown in Table 1 and in Figure 2. The completely unconstrained fit is the critical one. Note that the periods are not statistically different. However, the \dot{P} term for the BJD data is consistent with zero. For the historical data, the consistency with zero lies just inside the 90% contour, suggesting at this point at best marginal evidence for a changing period. Note, however, the magnitudes of the two \dot{P} terms: $\sim 4 \times 10^{-10}$ (BJD) vs $\sim 2 \times 10^{-12}$ (HJD).

We acknowledge that our ‘solution’ is *not* the best way to address this problem. The correct approach would convert the original JD times to BJD times. That study lies outside the scope of this paper because we lack the original JD times. Our approach demonstrates the increasing necessity of converting *all* times to a consistent reference frame, as noted by Eastman et al. (2010), because the precision is necessary to assess the possibility of changing periods. Given the results in Table 1 and the contours in Figure 2, it is possible a \dot{P} term exists but, at this point, is not supported by the data. This conclusion does not affect any of the remainder of this paper.

3. THE LIGHT CURVES

3.1. Overall Light Curve and Primary Eclipse Behaviors

Figure 3 shows the complete, filtered data sets at 1-minute cadence using the *K2* flux values (a, b = set 1, 2).

The points appearing near a flux level of $\approx 13,000$ are the bottoms of the primary eclipse. The denser band of points falling ≈ 5000 counts below the upper-most points of the light curves at all phases represent the bottoms of the secondary eclipses. Two arrows in each figure point to these bottom points, respectively.

That the primary eclipse drops the light to a nearly constant value tells us that the brightness variations are not visible during the eclipse. That behavior also shows that uneclipsed accretion structures (i.e., the outer portions of the disk and the stream) do not vary much in location, shape, or brightness from eclipse to eclipse.

In contrast, the light remaining at the bottom of the secondary eclipse is highly variable on time scales of days to weeks, and these changes track the changes outside eclipses. This implies that the day-week variability in AC Cnc arises in some combination of the inner portions of the accretion disk, the inner accretion stream, or the inner hemisphere of the secondary star. This is similar to the conclusions of Dmitrienko (1995) for the location(s) of variability in AC Cnc, based on the behavior outside and in the middle of eclipses.

Table 2 lists, and Figure 4 shows, the primary eclipse half-widths at half-maximum across both *K2* data sets. These widths are nearly constant at ~ 0.094 in phase – the median and mean values differ slightly: median: 1:0.0952 vs mean: 1:0.0932 and 2:0.0943 vs 2:0.0929. Within the

uncertainties, however, these are identical. The half-width start phases have a mean and median of 1:0.051 and 1:0.052 and 2:0.052 and 2:0.052, respectively. The corresponding end phase values are (mean, median) 1:0.042 and 1:0.043 and 2:0.041 and 2:0.042, respectively. Within the uncertainties, the two sets of mean and median values are also identical. The difference between the start and end phase may indicate a slightly asymmetric brightness distribution within the disk.

We note that there are essentially zero pre-eclipse ‘bright spots’ as sometimes observed in nova-like CVs (e.g., Warren et al. (2006); Dhillon et al. (2013)). Of particular note is the lack of pre-eclipse brightening before the rise of or during the bursts.

Finally, comparing the two data sets leads to two different descriptions: data set 1 shows a nearly-continuous variability in total light while data set 2 shows nearly constant total light. Interestingly, data set 2 has a mean out-of-eclipse level of $\sim 28K$ counts while data set 1’s mean is $\sim 23K$ counts. We can not make too much of this observation as we lack a sufficiently large data set to place those numbers in context.

3.2. Stunted Outbursts

Both data sets exhibit what appear to be stunted outbursts, as indicated by the labels. We compare their properties to the literature on stunted bursts in greater detail in the next section.

Figure 5 shows expansions of two sections of the data set 1 light curve at orbits away from an outburst (a) and on the rise of the larger burst (b). The expanded regions are indicated by the boxes in Figure 3(a). These are roughly representative of the range of behavior in both data sets.

We note that burst 2 appears to distort the eclipse ingress, shortening it from phase ~ 0.95 to $\sim 0.97 - 0.98$ as is visible in Fig. 4(a). Curiously, there is little apparent effect from burst 1 on the light curve. Burst 3, while not complete, also appears to decrease the ingress time near the peak of the burst.

Figure 6(a) shows a fully-phased light curve of data set 1 and 6(b) of data set 2. For data set 1, the heavy band in the center of the cloud of points is essentially the ‘mean’ light curve. The complete range for non-eclipse phases is $\approx 22K$ counts to $\approx 38K$ counts which corresponds to ~ 0.6 mag. Of that 0.6 mag, ≈ 0.4 represents the burst and the remaining ≈ 0.2 mag represents variations of the mean light curve. For data set 2, a similar description holds.

Excursions below the mean are largely due to the dip that follows Burst 2 (which can be seen in Figure 3(a) at orbits $\sim 1 : 200 - 215$). Such outburst/dip pairs are occasionally seen in other NL CVs having stunted outbursts, as noted in Honeycutt et al. (1998) and Honeycutt (2001). Dips following stunted outbursts have also been documented in *Kepler* photometry of KIC 9406652 (Gies et al. 2013), V523 Lyr (Mason & Howell 2016), and KIC 9202990 (Ramsay et al. 2016).

Figure 6 is useful to demonstrate the excursions from a mean behavior. But plotting all 246+169 light curves makes it impossible to follow a specific light curve. In Figure 7, we plot the light curves in blocks of ten. We immediately are able to pick out the orbits during which the stunted outbursts originated (orbits $\approx 1:11-30$ for burst 1;

TABLE 1
FITS FOR ECLIPSE EPHEMERIS

Quantity	\dot{P} -constrained		Period Constrained		All Unconstrained	
	Value	Uncertainty	Value	Uncertainty	Value	Uncertainty
	Historical times (HJD)		Historical times (HJD)		Historical times (HJD)	
Time-zero ^a	44290.30768	$\pm 3.1e-4$	44290.30768	$\pm 3.1e-4$	44290.30769	$\pm 3.1e-4$
Period	0.300477599	$\pm 5.0e-8$	0.300477600	$\pm 5.0e-8$	0.300477599	$\pm 5.0e-8$
\dot{P}	-4.3e-12	$\pm 2.1e-12$	-4.3e-12	$\pm 2.1e-12$	-4.3e-12	$\pm 2.1e-12$
	<i>K2</i> C05+C18 (BJD)		<i>K2</i> C05+C18 (BJD)		<i>K2</i> C05+C18 (BJD)	
Time-zero ^a	57139.32172	$\pm 1.2e-4$	57139.32170	$\pm 1.2e-4$	57139.32156	$\pm 2.2e-4$
Period	0.300477441	$\pm 4.7e-8$	0.30047862	$\pm 1.5e-6$
\dot{P}	-4.5e-11	$\pm 1.7e-11$	-3.07e-10	$\pm 3.8e-10$

^aTime zero is JD - 2,400,000. Uncertainties are 90% confidence limits.

TABLE 2
MEDIAN ECLIPSE HALF-WIDTHS

Eclipse	Data Set 1			Data Set 2		
	Phase In ^a	Phase Out ^a	Width	Phase In ^a	Phase Out ^a	Width
Primary	-0.0525 \pm 0.0005	0.0430 \pm 0.0004	0.0952 \pm 0.0013	-0.0525 \pm 0.0008	0.0418 \pm 0.0004	0.0943 \pm 0.0017
Secondary	-0.0605 \pm 0.0018	0.0612 \pm 0.0022	0.1217 \pm 0.0057	-0.0650 \pm 0.0027	0.0601 \pm 0.0028	0.1247 \pm 0.0078

^aAll phases listed in the table are relative to phase 0.5.

\approx 1:161-190 for burst 2; and orbits \approx 2:151-160 for burst 3). We also can identify the orbits during which the dip occurred (orbits \approx 1:201-220).

3.3. Secondary Eclipses

AC Cnc also exhibits secondary eclipses. Table 2 also lists the widths and ingress/egress phases for the secondary eclipses. Figure 8 shows the eclipse widths versus orbit number for pointings 1 and 2. As one might expect, there is considerable scatter in the widths stemming from the scatter in the ingress and egress phases. The two data sets look very similar, however. We do not see any orbit-dependent behavior related to the bursts. It is difficult to interpret the secondary eclipse behavior given that we do not know the exact source of the eclipsed light.

3.4. Summary

As a summary of this section on the light curves, we note the following in these plots:

- the primary eclipses of both data sets are completely centered on phase 0 to a high degree.
- with the exception of the stunted burst eclipses, the eclipse ingresses and egresses of essentially all of the orbits occur at the same phases. Note in particular that this behavior occurs even when the out-of-eclipse phases are relatively spread in counts (e.g., eclipses 1:41-50, 1:71-80);

- essentially *none* of the light curves reveal a significant pre-eclipse bright spot, especially before and during the stunted bursts;
- the secondary eclipses are more variable than the primary eclipses as one would expect given the nature of the eclipsed and eclipsing sources.

4. STUNTED OUTBURSTS: PROPERTIES

Stunted outbursts were first described by Honeycutt et al. (1998) based on \sim 6.5 years of data covering old novae and novalike systems. The bursts likely represent the actual state of affairs of CVs that have been described as in ‘continuous outburst.’⁴ Honeycutt et al. noted that these systems revealed ‘repetitive \sim 0.6 mag bursts, sometimes accompanied by \sim 0.6 mag dips.’ They reported detecting stunted bursts in about \sim 20% of the monitored systems. More recently, Mason & Howell (2016) note that the stunted burst behavior resembles the anomalous Z Cam behavior described by Simonsen (2011)⁵.

The outbursts of AC Cnc visible in the *K2* data set stand out for two reasons: first, they rise above the variability of the light curve with significant width relative to other variations. The mean light level is \approx 27-30K counts; the first burst rises to \sim 35K counts and the second to \sim 38K counts; the third burst rises to at least 38K counts.

Second, the three bursts are delineated by the *bottoms* of the primary eclipses (green lines in Figure 3): the eclipse minima lie at an essentially constant 12.6K counts, to a

⁴ That phrase appears to have first been used by E. Guinan for an IUE proposal (Guinan 1981).

⁵ As an editorial comment by the authors, we do not object to the connection, but if all CVs showing stunted bursts are called anomalous Z Cam CVs, the sheer numbers of objects calls into question the use of the adjective ‘anomalous.’ For this reason, in this paper we retain ‘stunted’ to describe the behavior.

high precision, *except* during the bursts, when the minima in the bursts only drops to ~ 13.5 K counts. That comment is not to suggest that the eclipse depth changes, but that ≈ 0.1 mag of the extra light is not eclipsed and that this only appears to occur in the bursts. Measuring from a mean peak to the bottom of the eclipse, bursts 1 and 2 cover 1.05 and 1.14 mag respectively, while the ‘bumps’ at orbits $\sim 1:60$ and $\sim 1:85$ are 0.95 and 0.98 mag, respectively. While burst 3 is incomplete, we still see the eclipse bottoms increase to ~ 13 - 14 K counts at roughly the burst peak.

Fitting bursts 1 and 2 for FWHM and amplitude, we obtain FWHM values of 3.4 ± 0.2 and 7.6 ± 0.4 days ($= 11.3 \pm 0.66$ and 25.3 ± 1.33 orbits, respectively) and amplitudes of ≈ 0.42 and 0.36 mags for AC Cnc. From ground observations, Honeycutt et al. (1998) measured an amplitude range of ≈ 0.4 to ≈ 0.75 mag and FWHM values from ≈ 4 - 7.5 days. The values for the two *K2* bursts fall within the envelope of ground observations of all stunted bursts (Figure 9). The *K2* AC Cnc points are shorter in duration than the mean of all AC Cnc ground observations, most likely because the ground data lack the time resolution necessary to define the FWHM as cleanly as is possible in the *K2* data. As burst 3 is incomplete, we do not include it. We note, however, that the FWHM and amplitude are at least similar to the values for burst 2.

The two different stunted outburst widths (~ 3.4 and ~ 7.6 days) seen in this *K2* data are suggestive of AC Cnc having two characteristic durations, which we call ‘normal’ and ‘extended’, respectively. The statistics are admittedly quite poor but the idea is supported by the behavior seen in dwarf novae. In most well-observed dwarf nova, the distribution of outburst widths is bimodal, with a pair of well-defined peaks separated by (typically) 4 to 8 days. Hack et al. (1993) compiled histograms of a number of dwarf novae showing this effect. Examples include X Leo Saw (1982), U Gem Isles (1976), Z Cam Petit (1961), EM Cyg Brady & Herczeg (1977) and Szkody & Mattei (1984), and SS Cyg Martel (1961). The phenomenon was modeled in SS Cyg by Cannizzo (1993) using the accretion disk limit cycle model for the outburst mechanism. If the suggestion of a bi-modal distribution of outburst widths is born out for AC Cnc, then the outbursts in dwarf novae and the stunted outbursts in novalike CVs may be related in interesting ways. To address this possibility, we would need multiple stunted bursts obtained with sufficient precision to discern whether a difference in burst width actually exists. On the basis of the measured *K2* widths, the bursts differ, but in comparison to stunted bursts measured from the ground (e.g., Figure 9), we can not infer a difference. It remains an intriguing possibility to be resolved with future (robotic?) observations.

5. DISCUSSION

Uninterrupted observations of CVs allow us to see an accreting system in its ‘orbit-to-orbit’, or ‘ordinary’, life. With a sufficiently broad range of CVs observed in that manner, disk modelers would have a clear set of data to test not only ‘snap shot’ physics but also the evolution of a model. The observations presented here of AC Cnc demonstrate that potential. There are only a handful of additional eclipsing CVs in the *Kepler* and *K2* datasets,

all of which are dwarf novae: the SU UMa DN V477 Lyr (Ramsay et al. 2012); DN KIS J192748.53+444724.5 (Scaringi et al. 2013; Littlefair et al. 2014); SU UMa DN CRTS J035905.9+175034 (Littlefield et al. 2018)), and the C18 data set of SU UMa DN SDSS J081256.85+191157.8 (Schlegel & Honeycutt 2019, in preparation).

That the bursts present in the *K2* data match observations obtained from the ground confirms that the *K2* outbursts may be identified as stunted bursts. In contrast to the ground observations, in which the bursts are usually defined by a handful of data points, *K2* reveals the bursts in exquisite detail. The single dip following burst 2 also matches the properties of the dips described in Honeycutt et al. (1998).

As noted previously, the primary eclipses are essentially constant in width, except for small changes during the peaks of the bursts. This implies that extra light spills out from behind the secondary during primary eclipse. Given the inferred inclination of the system (75.6 ± 0.7 , Thoroughgood et al. (2004)), enhanced accretion disk emission or a wind associated with a stunted burst could easily explain the difference.

In contrast, the secondary eclipses demonstrate significant variability. If we adopt 22.5K counts as a very approximate ‘mean’ for data set 1, then there are excursions of $+0.41$ mag and -0.27 from that value. These variations are not present in the background, so can not be attributed to other objects contaminating the *K2* field-of-view.

The secondary eclipse behavior essentially tracks the overall light curve (q.v., Figure 3), suggesting that mass transfer explains the variations. Yet the AC Cnc *K2* data also suggest that mass transfer variations are not the explanation of stunted bursts: we do not see enhanced brightening at the stream impact point prior to the stunted bursts.

In a typical CV model, we would attribute the variations to one or more of three sources: the L_1 -facing hemisphere of the secondary, mass transfer stream + impact point, or accretion disk. Any one or all of these sources could contribute to the AC Cnc secondary eclipse variations, leaving us in a similar position as that of Robertson et al. (2018). In that paper, the stunted bursts the authors observed in UU Aqr confidently led them to conclude that mass transfer via a blobby stream explained the stunted burst behavior. But they were equally acquainted with other systems strongly suggesting accretion disk instabilities as explanations for stunted bursts. The slight difference in inclination of UU Aqr ($78^\circ \pm 2^\circ$ (Baptista et al. 1994)) vs AC Cnc (75.6 ± 0.7 (Thoroughgood et al. 2004)) is too small to have a large impact on the interpretation of the data.

One must, however, also keep in mind that the eclipsing body for the secondary eclipse is the accretion disk and associated structures. Portions of the eclipsing body must be optically thick to produce a ≈ 0.25 mag deep secondary eclipse. If the optical depth of the accretion disk changes, however, due to variable accretion, then the depths of the secondary eclipses will also vary. The lack of pre-eclipse bright spots for AC Cnc appears to eliminate the stream and impact point as sources of the variations, leaving the facing hemisphere of the secondary, optical depth changes of the disk, or enhanced structure in the disk as possible explanations. For a ≈ 0.25 mag change, an enhancement in

the number density or in a small change in the disk structure, e.g., an enhancement in the disk rim, by 10-20% for number density and path length could account for the secondary eclipse variations. To quantify this more concretely will require detailed fitting of each eclipse curve. Such a study is planned but lies outside the scope of the current paper.

We are also left with an additional intriguing question: at exactly what point does an enhancement in the disk's light become a stunted outburst? Our question really boils down to the physics of the disk: can we really suggest that stunted burst 1 differs significantly from the three increases in flux centered on orbit numbers $\sim 1 : 60$, $\sim 1 : 85$, and $\sim 1 : 125$? One can argue that stunted burst 1 has a faster rise time and that property defines a burst. But the slope leading into the rise in stunted burst 2 (orbit numbers $\sim 1 : 150 - 160$) is very similar to the slope leading into the peak of the non-burst around orbit numbers $\sim 1 : 50 - 55$. What has occurred to lead to a burst, stunted or not, in one case and not the other? The bursts are clearly set off by the primary eclipse minima, illustrating that extra light is present, but what has changed? Based on the data set in hand, we do not have an answer.

6. SUMMARY

We described two pointings of the novalike CV AC Cnc using the *K2* satellite during Campaigns 5 and 18. The data cover nearly 100% of a continuous 1-minute sequence of

observations over 74 days for data set 1 and about 50 days for data set 2. The eclipse timing defines an ephemeris statistically consistent with prior definitions but provides *at best* marginal evidence for a period change – directly countering a claim in the published literature. The light curves reveal two complete, and one partially observed, stunted outbursts. The properties of the stunted bursts match those obtained from ground observations of nova-like CVs. The *K2* data fill in the behavior of the stunted bursts, showing a continuously varying evolution of the disk.

Facility: Kepler2

7. ORCIDS

EMS: 0000-0002-4162-8190; RKH: none

We thank the anonymous referee for comments that improved this paper. This paper includes data collected by the Kepler mission during its revamped K2 mission – specifically, Campaigns 5 and 18. Funding for the Kepler mission is provided by the NASA Science Mission Directorate. This research also made use of NASA's Astrophysics Data System. This research also make use of the software package PyKE (Still & Barclay 2012) distributed by the NASA *Kepler* Guest Support office. This work was supported by Kepler2 Grant GO3-4104Z and the Vaughan Family Professorship.

REFERENCES

- Baptista, R., Steiner, J. E., & Cieslinski, D. 1994, *ApJ*, 433, 332
 Brady, R. A., & Herczeg, T. J. 1977, *PASP*, 89, 71
 Cannizzo, J. K. 1993, *ApJ*, 419, 318
 Dhillon, V. S., Smith, D. A., & Marsh, T. R. 2013, *MNRAS*, 428, 3559
 Dmitrienko, E. S. 1995, *Astr. Lett.*, 21, 171
 Dmitrienko, E. S. 1991, *IzKry*, 83, 131
 Downes, R. A. 1982, *PASP*, 94, 950
 Eastman, J., Siverd, R., Gaudi, B. S. 2010, *PASP*, 122, 935
 Gies, D. R., Guo, Z., Howell, S. B., Still, M. D., Boyajian, T. S., Hoekstra, A. J., Jek, K. J., LaCourse, D., Winarski, T. 2013, *ApJ*, 775, 64
 Guinan, E. F. 1981, IUE Proposal ID #CVDEG
 Hack, M., Ladous, C., Jordan, S. D., et al. 1993, NASA Special Publication, 507
 Honeycutt, R. K. 2001, *PASP*, 113, 473
 Honeycutt, R. K., Robertson, J. W., & Turner, G. W. 1998, *AJ*, 115, 2527
 Howell, S. B., Sobek, C., Haas, M., Still, M., Barclay, T., Mullaly, F., Troeltzsch, J., Aigrain, S., Bryson, S. T., Caldwell, D., Chaplin, W. J., Cochran, W. D., Huber, D., Marcy, G. W., Miglio, A., Najita, J. R., Smith, M., Twicken, J. D., & Fortney, J. J. 2014, *PASP*, 126, 938
 Isles, J. E. 1976, *Journal of the British Astronomical Association*, 86, 327
 Kepler Data Characteristics Handbook (KSCI-19040-004, dated 31 May 2013)
 Kinemuchi, K., Fanelli, M., Pepper, J., Still, M., & Howell, S. B. 2012, *PASP*, 124, 963
 K rding, E. G.; Knigge, C.; Tzioumis, T.; & Fender, R. 2011, *MNRAS*, 418, L129
 Kreiner, J. M. 2004, *ActaAstron*, 54, 207
 Kurochkin, N. E. & Shugarov, S. Yu 1980, *Astr. Tsirk.* 1114
 Kurochkin, N. E. & Shugarov, S. Yu 1981, *Astr. Tsirk.* 1154
 Littlefair, S. P., Dhillon, V. S., G nsicke, B. T., Bours, M. C. P., Copperwheat, C. M., & Marsh, T. R. 2014, *MNRAS*, 443, 718
 Littlefield, C., Garnavich, P., Kennedy, M., Szkody, P., & Dai, Z. 2018, *AJ*, 155, 232
 Martel, L. 1961, *Annales d'Astrophysique*, 24, 267
 Mason, E. & Howell, S. B. 2016, *A&A*, 589, 106
 Patterson, J. 2012, *JAVSO*, 40, 240
 Petit, M. 1961, *Asiago Contrib* 119, 31
 Provencal, J. L., Shipman, H. L., Montgomery, M. H., & WET Team 2014, *Contr. of Astron. Obs. Skalnat Pleso*, 43, 524
 Qian, S.-B.; Dai, Z.-B.; He, J. J.; Yuan, J. Z.; Xiang, F. Y.; & Zejda, M. 2006, *A&A*, 466, 589
 Ramsay, G., Hakala, P., Wood, M. A., Howell, S. B., Smale, A., Still, M. D., & Barclay, T. 2016, *MNRAS*, 455, 2772
 Ramsay, G., Canizzo, J. K., Howell, S. B., Wood, M. A., Still, M., Barclay, T., & Smale, A., 2012, *MNRAS*, 425, 1479
 Robertson, J. W.; Honeycutt, R. K.; Henden, A. A.; & Campbell, R. T. 2018, *AJ*, 151, 61
 Saw, D. R. B. 1982, *Journal of the British Astronomical Association*, 92, 220
 Scaringi, S., Groot, P. J., & Still, M. 2013, *MNRAS*, 435, 68
 Schlegel, E. M.; Honeycutt, R. K.; Kaitchuck, R. H. 1984, *ApJ*, 280, 235
 Shugarov, S. Yu. 1981, *SovAstr*, 25, 332
 Simonsen, M. 2011, *JAAVSO*, 39, 66
 Still, M. & Barclay, T. 2012, *Astrophysics Code Library*, code ascl:1208.004
 Szkody, P., & Mattei, J. A. 1984, *PASP*, 96, 988
 Thoroughgood, T. D., Dhillon, V. S., Watson, C.A., Buckley, D. A. H., Steeghs, D., & Stevenson, M. J. 2004, *MNRAS*, 353, 1135
 Torbett, M. V. & Campbell, B. 1987, *ApJ*, 318, L29
 Warren, S. R., Shafter, A. W., Reed, J. K. 2006, *PASP*, 118, 1373
 Yamasaki, A; Okazaki, A; & Kitamura, M. 1983, *PASJ*, 35, 423

FIG. 1.— The distribution of $K2$ events on the pixels surrounding AC Cnc for data set 1. A light curve at each pixel shows the events detected by the given pixel. The area in dark gray is the standard area of events extracted for the target; the remaining white area shows the background and possible sources of contamination (the black square in the upper left is an unused pixel required by the FITS standard Kepler (2013)). The *lack* of events outside of the target area demonstrates that the data set is quite uncontaminated. The plot for data set 2 demonstrates the same conclusion and has not been included.

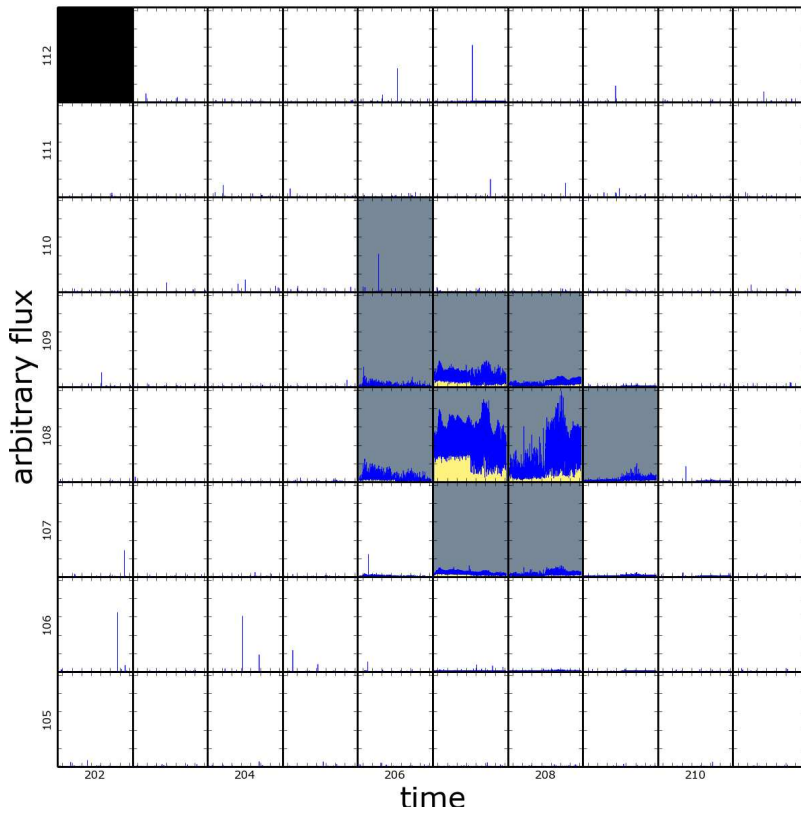


FIG. 2.— Contours for times of minimum: (a) historical period (HJD) vs K2-only period (BJD); and (b) $\dot{P}_{historical}$ vs \dot{P}_{K2only} , both from the unconstrained fit; and (c) historical period (HJD) vs K2 period (BJD) with \dot{P} equal for the two data sets. The lines in (c) indicate equal periods relative to the best-fit solution. Note that the horizontal and vertical scales differ in scale by 10x in (a).

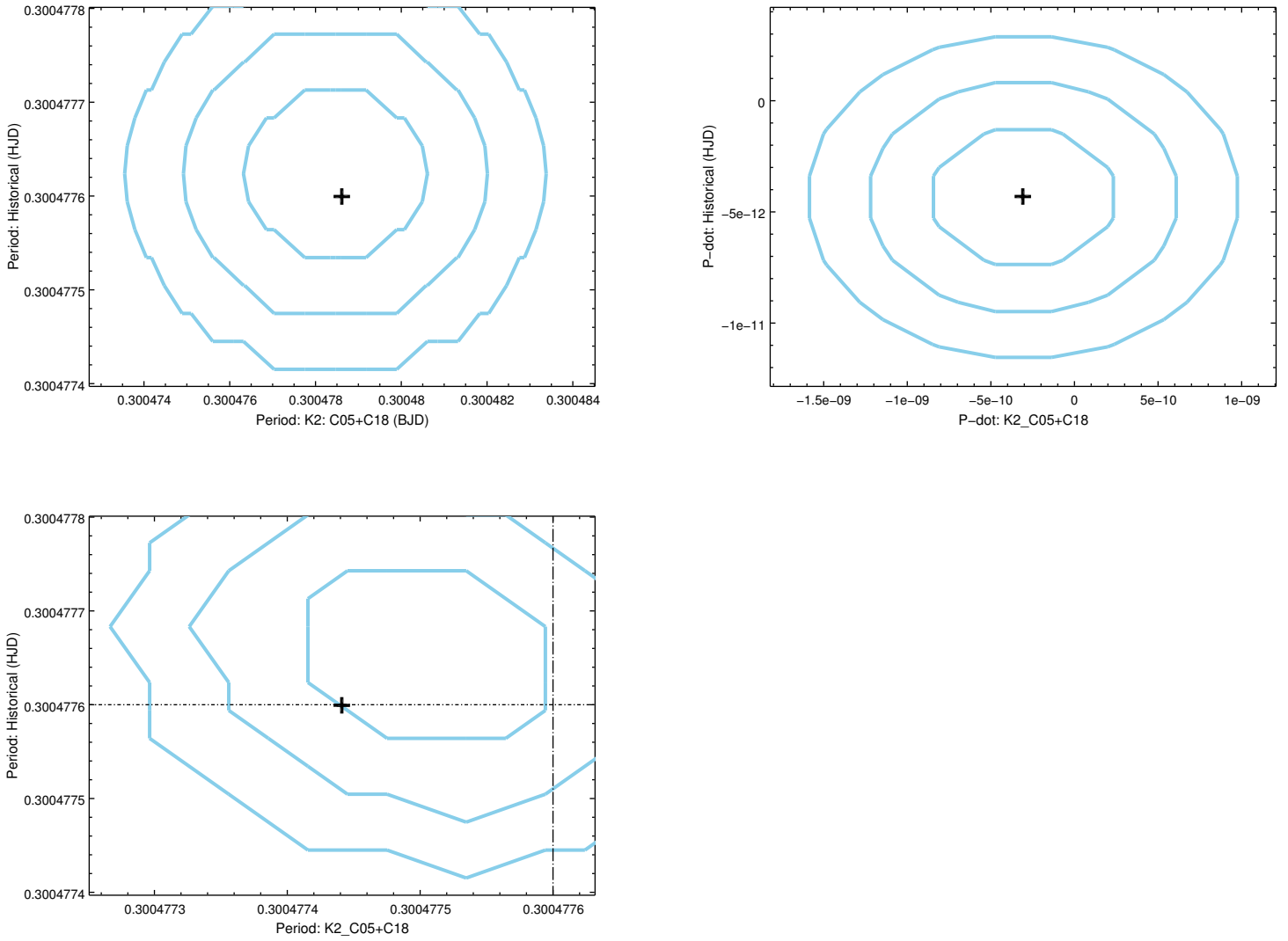


FIG. 3.— The complete *K2* light curve of AC Cnc. Note the bottoms of the primary and secondary eclipses in each light curve as delineated by the colored arrows. Also note the two stunted outbursts in data set 1 and the initial phases of burst 3 in data set 2. Phases are assigned based on the ephemeris listed in §2. The colored boxes are extracted and shown in Figure 5. The smooth line labeled ‘Background’ indicates the background counts boosted by a factor of 2. The green arrows (data set 1) and tilted line (data set 2) indicate the responses of the primary minima to the outbursts. (a) Data Set 1

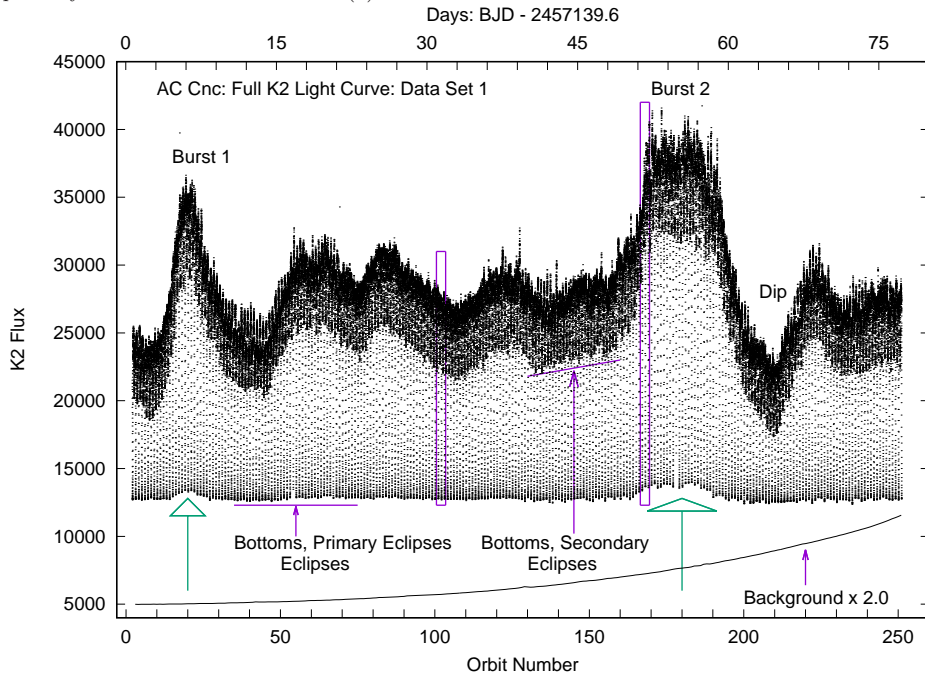


FIG. 3.— (b) The complete light curve for data set 2 showing a stunted burst cut off by the fuel pump ‘hiccup.’ A data gap exists at orbits 46 and 47. See the caption to (a) for complete details.

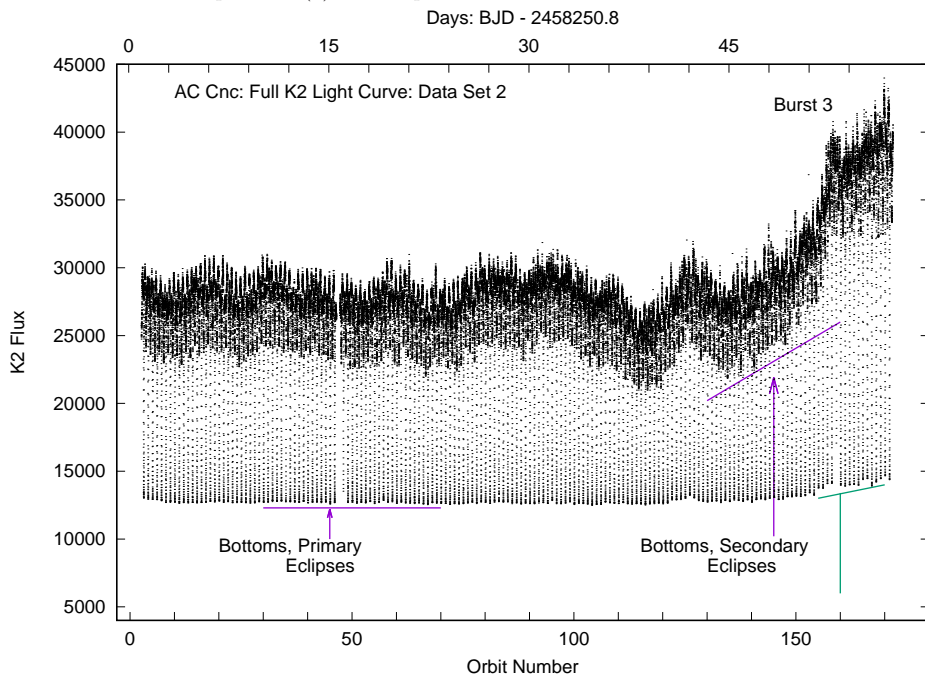


FIG. 4.— Primary eclipse half-width at half-maximum vs orbit number. The top plot shows the half width; the bottom shows the starting and ending phases. Each set of points also shows the median (blue line) and mean (gold line) values – for the starting phases, both median and mean are nearly identical; the half-width values are slightly separated: the median $\sim 0.0952 \pm 0.0009$ vs the mean $\sim 0.0932 \pm 0.0006$. The red rectangles indicate the orbits of bursts 1 (left) and 2 (right). (a) Data Set 1

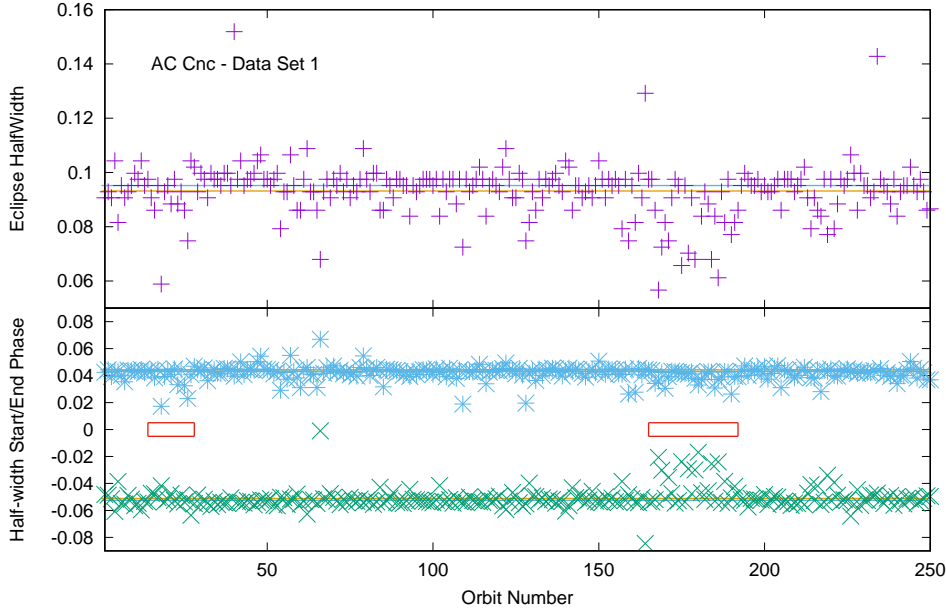


FIG. 4.— (b) Primary eclipse half-width for data set 2. The median value is 0.0943 ± 0.0122 vs. the mean value = 0.0929 ± 0.00094 . The red rectangle indicates the orbits of burst 3.

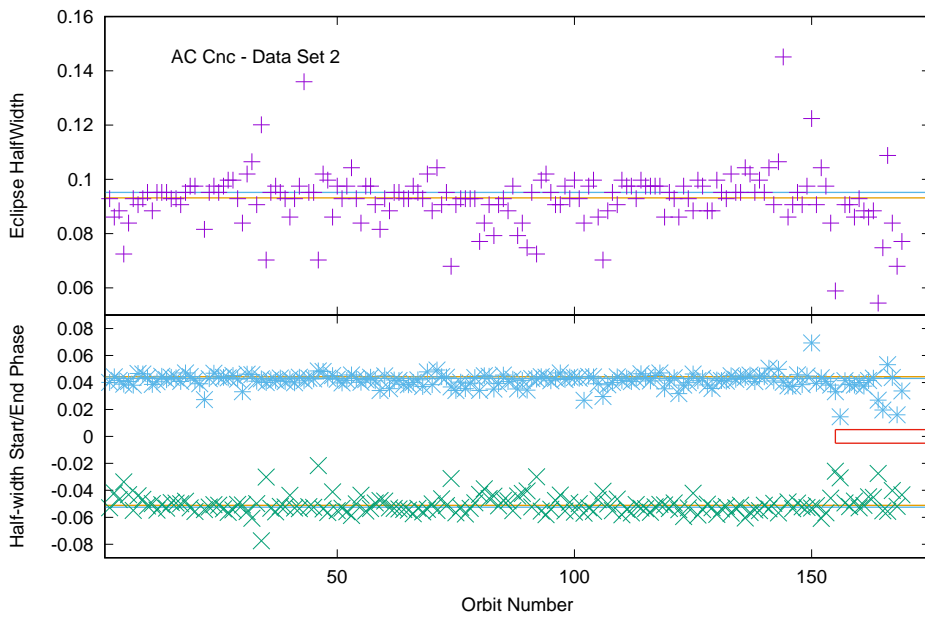


FIG. 5.— Orbital light curves for two selected portions of the light curve of Data Set 1 (Figure 3(a)) where the selections are marked by colored boxes: (left) orbits ~ 100.5 to 103.5 and (right) orbits ~ 171.5 to 174.5 . A short data gap typical of cosmic ray hits occurs just prior to eclipse at 168.7 .

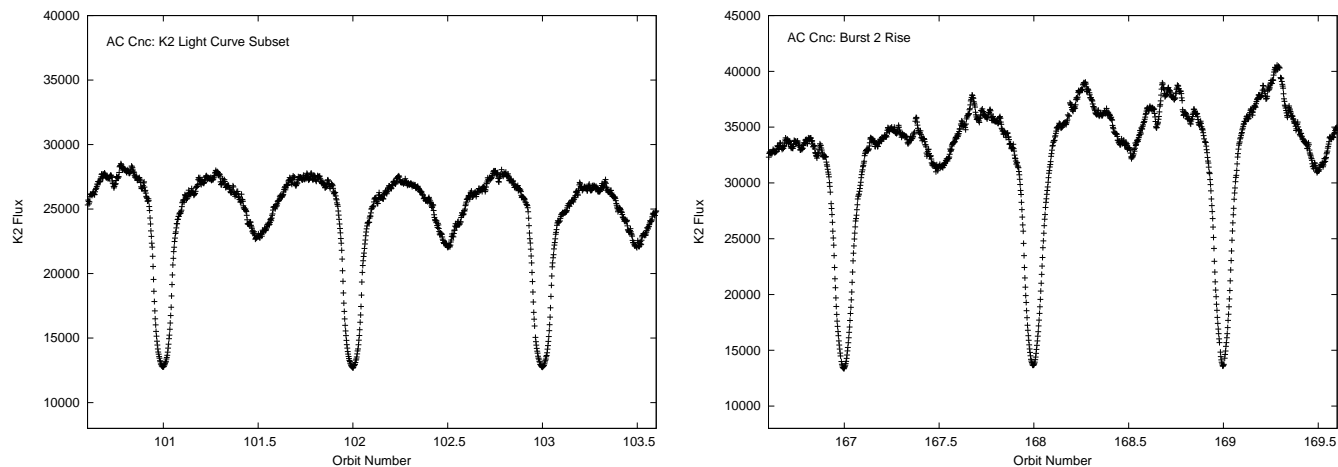


FIG. 6.— The fully-phased light curve of AC Cnc using a different color for each orbit. The primary and secondary eclipses are readily apparent as is pseudo ‘two-state’ light levels, ‘pseudo’ because of the essentially continuous nature of the variations. Given this behavior, sampling the light curve at frequencies typical of ground-based observatories could easily lead to an inference of ‘state changes’. (a) data set 1

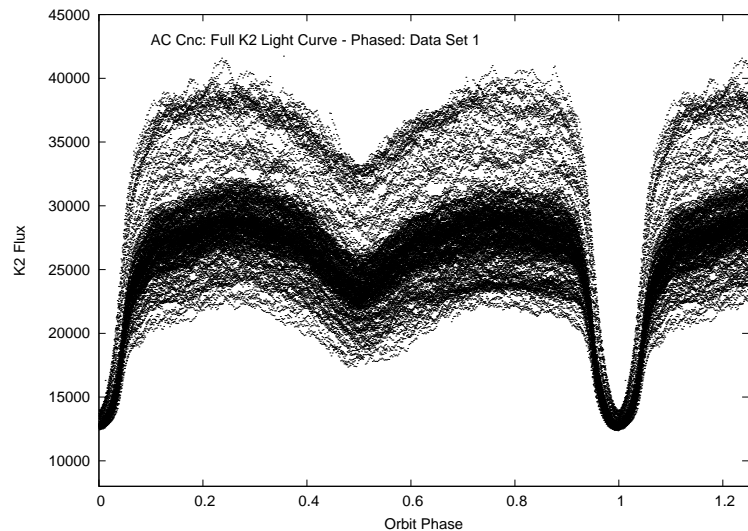


FIG. 6.— (b) The fully-phased light curve for data set 2. The cutoff of observations prevented catching the decline of the stunted burst. That makes the phased light curve resemble a state change. See the text for a longer discussion.

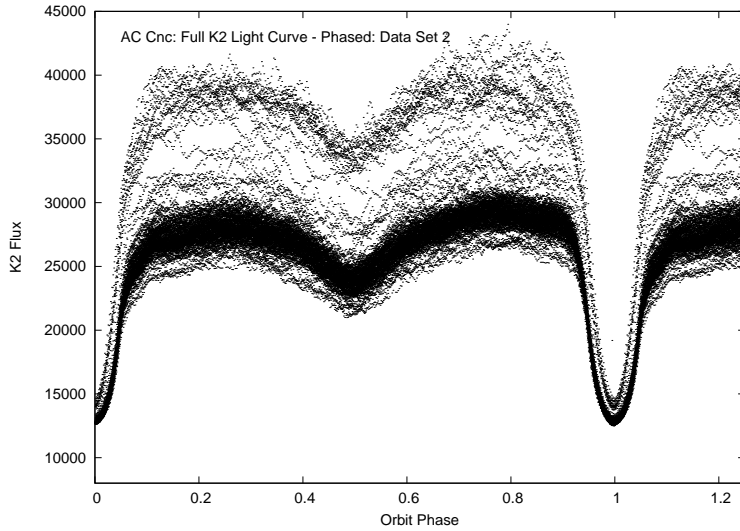


FIG. 7.— The complete set of light curves broken into 10-orbit blocks (the numbers inside each plot-let). The colors assigned to each light curve cycle through the same order for each plot-let, starting with black. The color order is most readily visible in the 11-20 plot-let (where the light curves are most affected by the stunted burst). (a) data set 1, orbits 1-150.

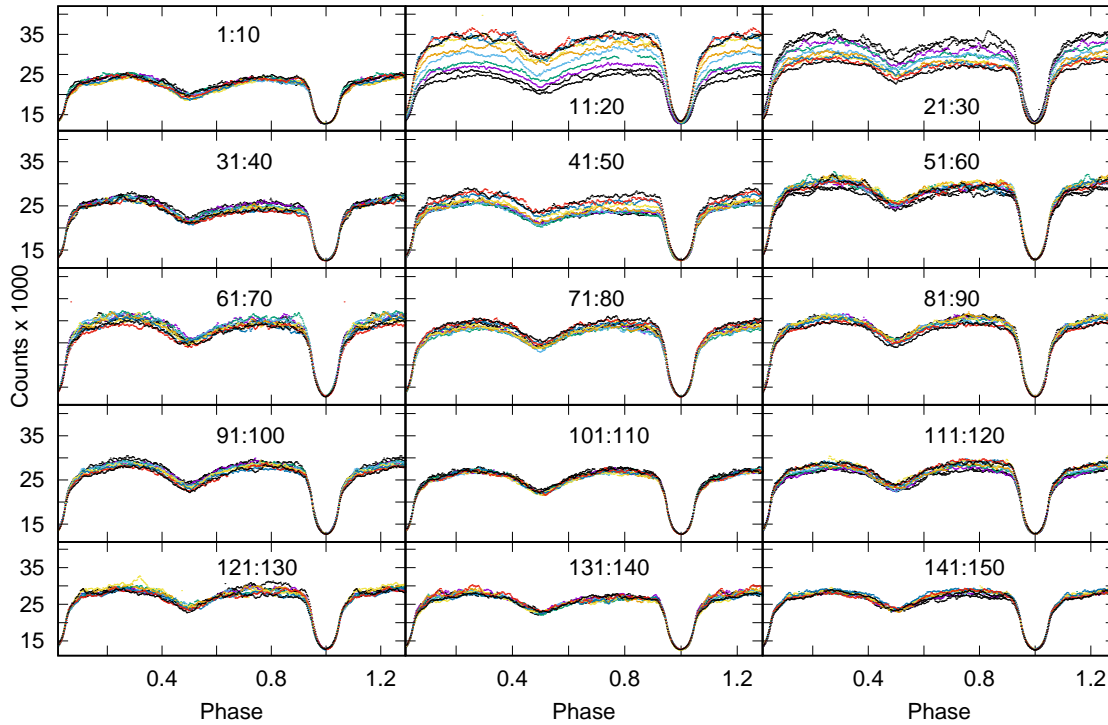


FIG. 7.— The complete set of light curves broken into 10-orbit blocks (the numbers inside each plot-let) (b) data set 1, orbits 151-246.

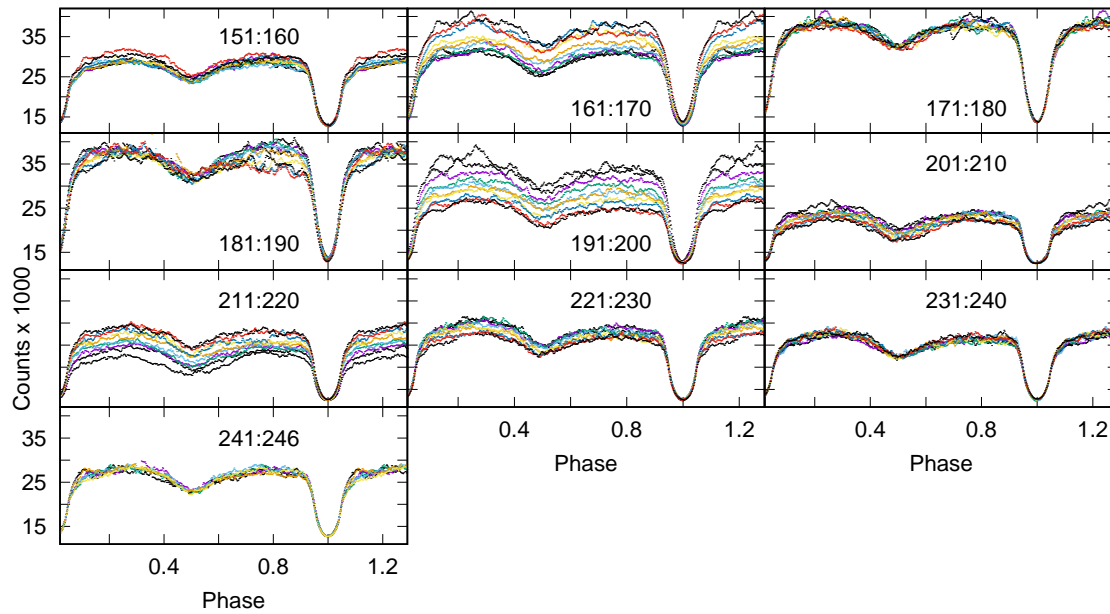


FIG. 7.— The complete set of light curves broken into 10-orbit blocks (the numbers inside each plot-let) (c) data set 2, orbits 1-120.

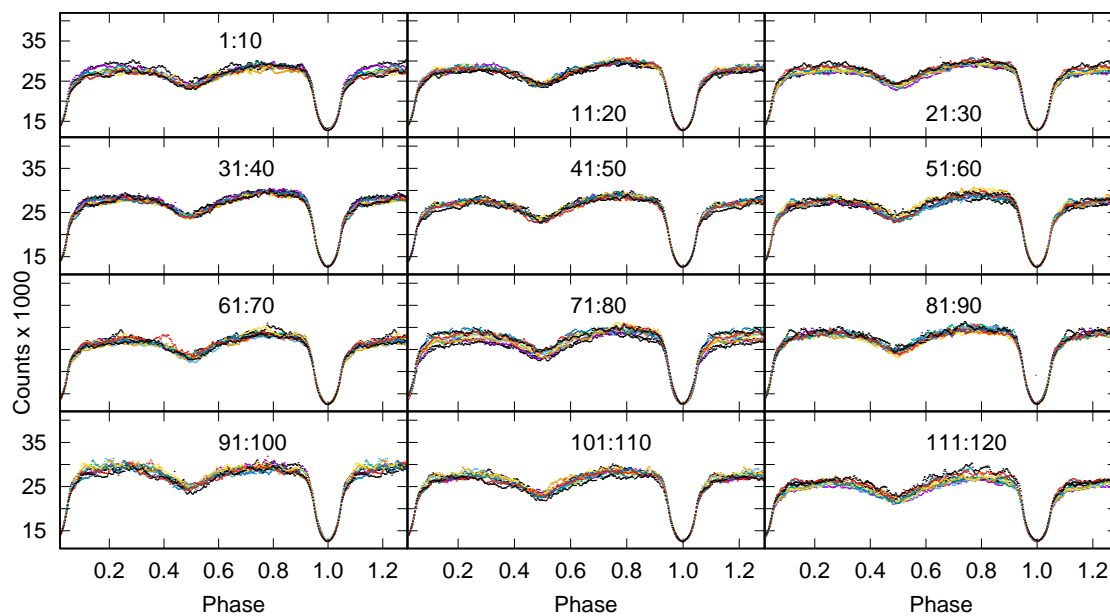


FIG. 7.— The complete set of light curves broken into 10-orbit blocks (the numbers inside each plot-let) (b) data set 2, orbits 121-171.

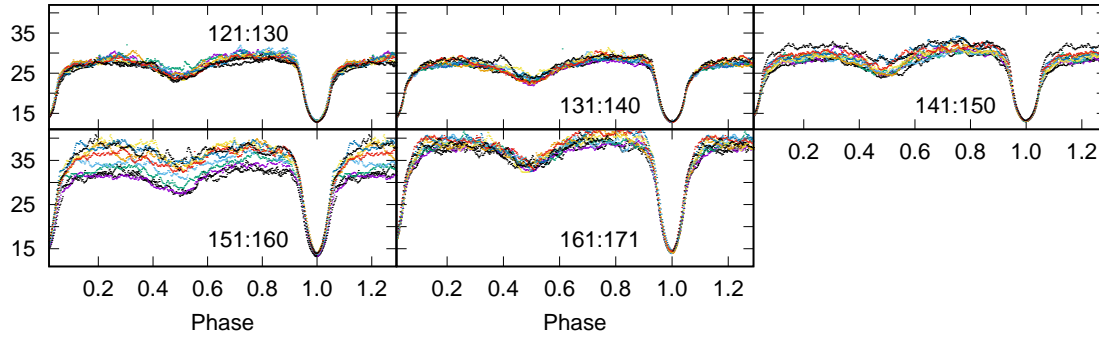


FIG. 8.— Secondary eclipse widths for the two data sets. (a) Data set 1.

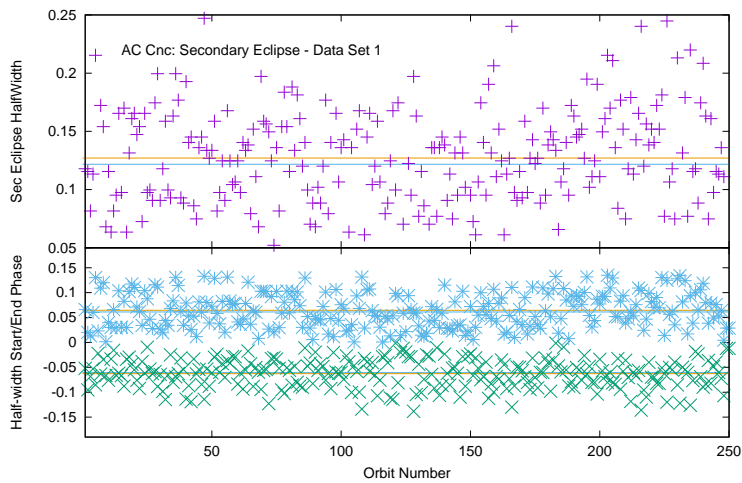
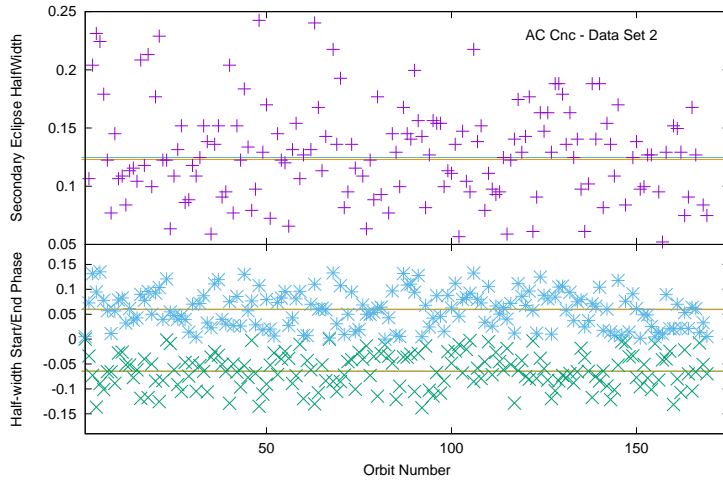


FIG. 8.— Secondary eclipse widths: (b) Data set 2.

FIG. 9.— A comparison of the amplitude and FWHM of stunted outbursts of the *K2* outbursts of AC Cnc during C05 with a number of cataclysmic variables, including ground (grd) observations of AC Cnc. Uncertainties are suppressed for visibility but are ~ 0.5 day (FWHM) and 0.05 mag in amplitude.